Journal of Constructional Steel Research 153 (2019) 209–221

Contents lists available at ScienceDirect

Journal of Constructional Steel Research

Experimental study of rigid connection of drilled beam to CFT column with external stiffeners

Nader Fanaie, Hossein Sadeghi Moghadam *

Department of Civil Engineering, K. N. Toosi University of Technology, Tehran, Iran

ARTICLE INFO

Article history:
Received 14 June 2018
Received in revised form 10 October 2018
Accepted 17 October 2018
Available online xxxx

Keywords:
Rigid beam to column connection
Concrete Filled Tube (CFT) column
T-shaped stiffener
Beam drilling
Reduced Beam Section (RBS)

ABSTRACT

This research is intended to investigate the behaviour of rigid connection of steel beam to CFT column with external T stiffeners. However, the investigations have shown that the stress concentration in the location of stiffener groove welds to the beam flange and column web causes abrupt fragile failure leading to ductility reduction of the connection. In the current study, beam section is reduced using the method of drilling beam flange so as to diminish the stress concentration and increase the ductility. This method is much easier to fabricate compared to RBS (cutting with CNC machine) and more applicable for existing buildings as well. In this research project two series of analytical models with constant and variable holes are investigated to evaluate the effects of different parameters of drilling on the local behavior of connections. Finite element method using ABAQUS software has been employed for analyses. In another part of this survey, two full scale samples are selected out of the analytical models, and experimentally investigated. According to the obtained results, drilling the beam flange results in decrease in stress concentration in the connection location of stiffener to the beam and column. In addition, it decreases the probability of failure in the expected modes 1 (shear failure of T-shaped horizontal stiffener) and 2 (tension failure of T-shaped vertical stiffener in connection to the column web) and increase the ductility of connection. Moreover, such connections can be used in the intermediate as well as special moment resisting frames.

1. Introduction

Concrete and steel are the most common materials in the construction of structures, each of which has its own advantages. Concrete Filled Tube (CFT) columns combine the ductility of steel with stiffness of concrete. Such columns consist of a steel box inside of which is filled with concrete. CFT columns have excellent characteristics such as high bearing capacity in compression, bending, shear and torsion [1–3]. These columns are specific because of their high stiffness; therefore, they are by far the best choice for moment resisting frames. However, considering the internal concrete, the continuity plate in the rigid CFT connections interrupt pouring the concrete [4]. For eliminating the continuity plate, the researchers have suggested different alternatives which are still in theory and far from practice and implementation. Besides, the main objective of the designer is to design a cost-effective structure with appropriate performance.

Execution of end plate connection is difficult due to the existence of through bolts passing column. Construction of through beam connection is difficult as well because of the column cutting and disturbing for concreting [5]. Connections with the internal passing diaphragm is also difficult to fabricate because of the column cutting and limited space for concreting [6,7]. Therefore, the connections with stiffeners and external diaphragms are the best rigid ones for CFT columns. Among the rigid connections suggested for CFT columns, the ones with T- shaped stiffeners have more advantages such as simplicity fabrication, being cost-effective relatively, not cutting the column in the connection region, and not disturbing the column concreting. However, the stress concentration in the groove welds of stiffeners to the beam and column is one of the difficulties of these connections, which restricts their applications.

Refined nonlinear finite element model has been used by Brunesi et al. (2014) to account the influence of friction and relative slippage of components. Finite element models were developed by adopting isoparametric displacement-based (DB) solid elements to evaluate local stress/strain distributions. The classical von Mises yield criterion with combined isotropic and kinematic strain hardening was assumed to accurately reproduce the cyclic stress-strain relationship of the steel members. Linear fitting techniques were exploited to propose a conservative closed-form equation and quick rotational stiffness estimation in the connection systems [8].

Brunesi et al. (2015) developed a finite element model to evaluate partially-restrained bolted beam-to-column connections. Three-

* Corresponding author at: University of Technology, Civil Engineering Department, No. 1346, Vali-Asr Street, P.O. Box. 15875-4416, 19697 Tehran, Iran.
E-mail address: hsadeghi@mail.kntu.ac.ir (H.S. Moghadam).

https://doi.org/10.1016/j.jcsr.2018.10.016
0143-974X/

dimensional solid and one-dimensional fiber elements have been used in their study. The contact conditions included the combined effects of slip and friction, employing master-slave pairs. They showed that the advanced solid finite element models give more insight than equivalent mechanical idealizations. However computational time is increased by using the solid elements and run with parallel processing on multiprocessor computers is needed [9].

Nascimbene [10] proposed a finite element model for studying of two-dimensional arc structure. Simple three-node (9 degrees of freedom) and five-node (15 degrees of freedom) curved shear flexible beam elements have been developed by Nascimbene to avoid membrane and shear locking. Many problems have been solved to verify the proposed formulation [10].

Nascimbene expressed that transverse shear strain effect is an undesirable and unavoidable numerical effect. Shear locking phenomenon appears in a finite element model which is unable to represent zero shears in the elements on pure bending. Some solutions (discontinuous Galerkin methods and reduced integration) have been proposed to avoid numerical locking. Nascimbene developed a Based-Gauss-Mixed-Interpolation (BGMI) method to solve this issue. The nine-node element defined by Nascimbene has an appropriate convergence and yields accurate predictions, even with coarse mesh [11].

Kang et al. showed that T stiffeners can prevent pinching in hysteresis curves, and improve the behavior of the connection. However, the stress concentration observed at the corners of the column caused fracture in this region [12]. Shin et al. showed three failure modes for the connections with T stiffeners. These three modes are failure of the horizontal element of stiffener, failure of the vertical element of stiffener and failure with local buckling of beam flange, respectively. The first and second failure modes are brittle and undesirable but the third failure mode is ductile and desirable [13].

Kim et al., focused on reducing the stress concentration in the stiffeners and corners of HSS column using RBS beams [14]. Kang et al. studied the influence of geometric characteristics of horizontal and vertical elements of T stiffeners and modified the design equations. They also determined the effect of steel box thickness [15]. In addition, drilling the beam flange is a simple and economical method for reducing stress and plastic strain concentration at the interface of beam and column. This method can be applied to the existing structures. Tsai et al. studied 12 connections with different details of the beam to I-shaped and built-up box columns. They showed that by applying an appropriate hardening factor, drilling the beam flange caused the increase in plastic rotation capacity of the connection [16].

Lee et al. focused on increasing ductility, seismic improvement of existing welded connections, and reduction of stress concentration. They concluded that higher plastic rotation capacity can be achieved by RBS beam with staggered holes in comparison with a linear direction [17]. Vetr et al. examined two drilled specimens with different diameters subjected to cyclic loading. According to the results obtained by strain gauges, the fracture has occurred in the nearest holes to the column face which has experienced maximum strains. Therefore, in order to create uniform strains, more studies on the distances between the holes and their distances from the column face are suggested [18].

Kazerani et al. investigated different drilling parameters of the beam flange. For this purpose, 62 models of drilled beam connections to steel columns were modeled in ABAQUS software. The models were subjected to cyclic loading and push over analysis. They concluded that these connections had proper seismic behavior. However, they believed that more experimental studies were needed to ensure the performance of these connections [19].

This research focuses on the effect of drilling on the steel beam to CFT column connection to reduce the stress concentration in the groove welds and shift the plastic hinge away from the column face. Drilling of beam flange is one of the efficient methods for reducing the beam cross-section similar to RBS. Besides, it causes more extension and increase in the plastic hinge length and therefore provide higher flexural capacity in the beam. Besides, the behavior of T-shaped external stiffeners is discussed, and different details of beam drilling on this connection are investigated in this study. The equivalent plastic strain curves (PEEQ) and rupture index (RI) have been reported in the finite element model for more accurately assessing the groove welds. Then, two full scale specimens have been investigated experimentally to observe the real behavior of this type of connection and the obtained results are thoroughly reported in this study.

2. Analytical assessment of the connection

2.1. Modeling

The steel is modeled based on the von Mises yield criterion, considering the possibility of large deformations and nonlinear behavior of materials. Modulus of elasticity and Poisson's ratio of steel are assumed 210 GPa and 0.3, respectively. The kinematic hardening rule and concrete damage plasticity model has been used for modeling the steel and concrete, respectively. The model proposed by Susantha [20] has been used for the stress-strain relationship of concrete. This model has been suggested for composite steel sections filled with concrete and verified with numerous experimental specimens.

The number of elements in the finite element model is 4300 elements on average. For accurate modeling, solid elements are used for all the deformable components. 20-node quadratic brick with reduced integration (C3D20R) is used in the connection zone and 15-node quadratic triangular prism element (C3D15) is used for complicated areas such as stiffeners. Other components are meshed by 8-node linear brick elements (C3D8R) with reduced integration. Discrete rigid elements with 4-node is used for rigid plates at the end of beam and column. Static general step and direct equation solver with full Newton solution technique is chosen for analysis.

Shear locking occurs in first-order, fully integrated elements in ABAQUS which are subjected to bending. The numerical formulation of elements results rise of shear strains that do not really exist. Therefore, these elements are too stiff in bending. In this study, reduced integrated elements have been used to prevent shear locking. Furthermore, second-order isoparametric elements including the 8-node quadrilateral and the 20-node brick are used in the critical areas with more stress/strain.

Surface to surface contact type is used in ABAQUS with automatically smooth 3D geometry surfaces for contact between steel and concrete. Contact property contains tangential and normal behavior. Tangential behavior is defined by isotropic directionality and penalty friction formulation and normal behavior are defined according to hard contact pressure overclosure and penalty constraint enforcement method. Separation after contact is allowed for steel and concrete. Contact stiffness behavior is defined nonlinear. Besides, a tie constraint is defined between the rigid plates and the main model.

2.2. Model verification

To ensure the accuracy of analytical results, the finite element model has been verified with cyclic results of TSD120specimen examined by Shin et al. [21]. Fig. 1 presents the deformation of the analytical model and the experimental specimen of Shin et al. research. Moreover, comparison of analytical and experimental hysteresis curves is shown in Fig. 2. As seen, the analytical results are corresponded well with the experimental ones.

2.3. Connection design

In this study, analytical models are categorized into two sets. Column and beam dimensions are considered constant in each set, and beam is considered stronger in the second set of analytical models. The external T stiffeners are considered to transfer the forces from the

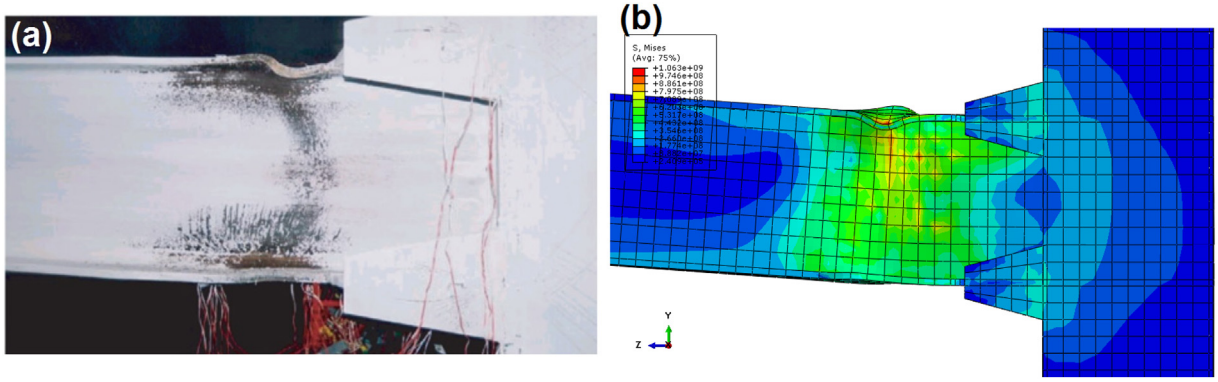

Fig. 1. Modeling for verification; a) TSD120experimental specimen [21]; b) finite element model.

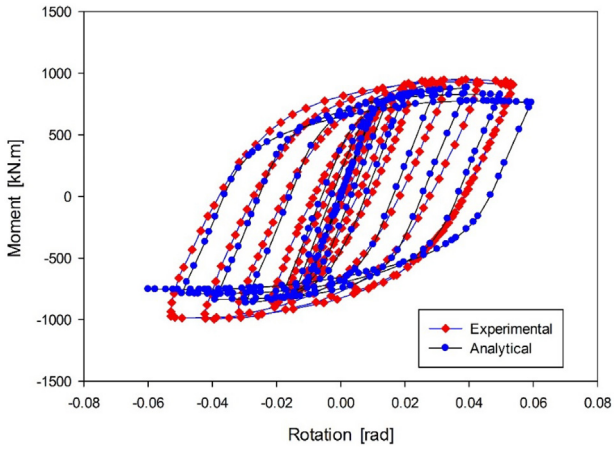

Fig. 2. Comparison of analytical and experimental hysteresis curves plotted for TSD120.

beam to column, so the continuity plates are not required in this connection. The T stiffener dimensions are constant in each model set. In fact, in the second model set, stronger stiffeners are used in accordance with the stronger beam. Connection design is carried out based on AISC specifications with necessary controls. Geometric dimensions of the T stiffeners are obtained based on the design method introduced in the previous researches [15,21–23], as presented in Table 1. In this table, L_s is the length of stiffener, W_{hs} is the width of horizontal element, and H_s is the height of vertical stiffener. Fig. 3 shows the T stiffener.

2.4. Material property and loading

Materials and elements nonlinearity is taken into account in the modeling. Material properties are summarized in Table 2. Concerning the fact that this study is analytical-experimental, material properties are obtained from the experimental tension tests of steel plates based on the ASTM E8/E8M-09 standard [24]. Cyclic loading tests are conducted according to SAC loading protocol [25]. One cycle is considered for each drift ratio in the analytical models.

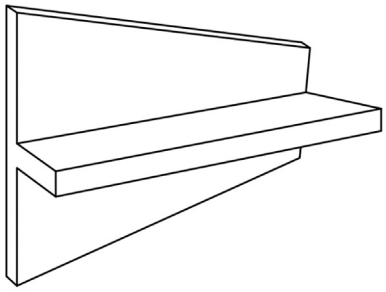

Fig. 3. T-shaped stiffener.

2.5. Hole-drilling with variable diameter

The hole diameter in the first model set is variable and thickness and width of beam flange are 15 mm and 180 mm, respectively. Moreover, thickness and height of the beam web are 8 mm and 300 mm, respectively. The column is a square Hollow Structural Section (HSS) with a width and thickness of 300 mm and 10 mm, respectively. In the analytical models, beam length and column height are considered as 2.5 m and 3 m, respectively.

The first set contains 19 models which TSF-1 is without hole-drilling. Geometric specification of the other 18 models are given in Table 3. In this table, L_d is the distance between holes, b is the distance between the first and last hole, D_{max} is the diameter of the biggest hole, and D_{min} is the diameter of the smallest hole.

Design of the holes in the first set of models is based on the simultaneous formation of plastic hinges at the drilled cross sections. According to the studies conducted by Vetr et al. [18], this caused an increase in the plastic hinge effective length and lead to a more uniform distribution of plastic strains along the reduced area compared to the RBS connection. In this models, with an increase in distance from the column, beam section modulus changes with adjusting the hole diameter considering the

Table 1
Geometrical specifications of T-stiffener in the first and second model sets (All dimensions are in mm).

Analytical models	Stiffener	L_s	W_{hs}	H_s	t
First set of analytical models	Vertical	230	–	160	10
	Horizontal	230	45	–	15
Second set of analytical models	Vertical	250	–	180	10
	Horizontal	250	45	–	15

Table 2
Results of steel tension test.

Location	Thickness (mm)	Steel type	F (MPa)	F_u (MPa)	Elongation (%)
Beam Web	8	ST37	303	382	31
Beam Flange and Horizontal Stiffeners	15	ST37	244	384	35
Vertical Stiffeners	10	ST37	295	415	33
CFT Column Plates	10	ST37	469	549	25

Table 3
Specifications of the first set of analytical models (All dimensions are in mm).

Model	Number of holes	Diameter of smallest hole (D_{min})	Diameter of biggest hole (D_{max})	Distance between the first and last hole (b)	Center to center distance of holes	$\frac{D_{min}}{b_f}$	$\frac{D_{max}}{b_f}$	$\frac{b}{d_b}$
TSDF-1	3	18	27	210	105	0.1	0.15	0.7
TSDF-2	3	27	36	210	105	0.15	0.20	0.7
TSDF-3	3	33	42	210	105	0.18	0.23	0.7
TSDF-4	4	18	27	210	70	0.10	0.15	0.7
TSDF-5	4	27	36	210	70	0.15	0.20	0.7
TSDF-6	4	33	42	210	70	0.18	0.23	0.7
TSDF-7	3	18	27	240	120	0.10	0.15	0.8
TSDF-8	3	27	36	240	120	0.15	0.20	0.8
TSDF-9	3	33	42	240	120	0.18	0.23	0.8
TSDF-10	4	18	27	240	80	0.10	0.15	0.8
TSDF-11	4	27	36	240	80	0.15	0.20	0.8
TSDF-12	4	33	42	240	80	0.18	0.23	0.8
TSDF-13	3	18	27	270	135	0.10	0.15	0.9
TSDF-14	3	27	36	270	135	0.15	0.20	0.9
TSDF-15	3	33	42	270	135	0.18	0.23	0.9
TSDF-16	4	18	27	270	90	0.10	0.15	0.9
TSDF-17	4	27	36	270	90	0.15	0.20	0.9
TSDF-18	4	33	42	270	90	0.18	0.23	0.9

Table 4
Diameter of holes in drilling the beam in the first set of analytical models.

Model	Hole diameter (mm)
TSDF-1, TSDF-7, TSDF-13	18–23-27
TSDF-2, TSDF-8, TSDF-14	27–31-36
TSDF-3, TSDF-9, TSDF-15	33–38-42
TSDF-4, TSDF-10, TSDF-16	18–22–25-27
TSDF-5, TSDF-11, TSDF-17	27–30–33-36
TSDF-6, TSDF-12, TSDF-18	33–36–39-42

reduction of beam moment. To this end, Eq. (1) is used:

$$\frac{M_1}{Z_1}=\frac{M_2}{Z_2}=\frac{M_3}{Z_3}=\frac{M_i}{Z_i} \quad (1)$$

In this equation, M_i's and Z_i's are bending moment and plastic section modulus in the i^{th} hole location on the beam flange, respectively. Based on Eq. (1), the hole diameters are obtained for analytical models. Table 4 presents the hole diameters for each model and Fig. 4 schematically shows hole drilling on the beam flange with four holes. To evaluate the effect of drilling on stress concentration, the amount of equivalent plastic strain (PEEQ) and von Mises Stress are investigated on lines AB and CD in the location of T stiffener groove welds to the beam and column, as shown in Fig. 5.

2.5.1. Effect of D_{max}/b_f ratio

The results show that an increase in the D_{max}/b_f ratio lead to decrease in the beam moment capacity. On the other hand, the amount of equivalent plastic strain (PEEQ) and von Mises stress decrease in the location of the stiffener groove welds to the beam and column. Fig. 6 shows a comparison between three analytical models with different hole diameters.

2.5.2. Effect of b/d_b ratio

In general, the results showed that reduction in moment capacity of models with four holes is greater than those with three holes. However, in the TSDF-17 and TSDF-18 models with four holes, the moment capacity is higher than that of TSDF-14 and TSDF-15 models with three holes. This should be noted that the distance between holes in the TSDF-17 and TSDF-18 models is more than that of TSDF-14 and TSDF-15 models. The amount of PEEQ in the groove weld point of stiffener to the beam and column increases with an increase in b/d_b ratio. Nevertheless, in the TSDF-17 and TSDF-18 models, the distance between holes is more significant compared to that of TSDF-14 and TSDF-15 models and the PEEQ amount increases in the location of groove weld of stiffener to the beam and column as the b/d_b ratio increases. With greater distance between holes in the TSDF-17 and TSDF-18 models compared to that of TSDF-14 and TSDF-15 models, the PEEQ amount decreases in the groove weld location. Fig. 7 indicates that with a decrease in the b/d_b ratio, plastic strain reduces in the edge of the horizontal stiffener and becomes more uniform.

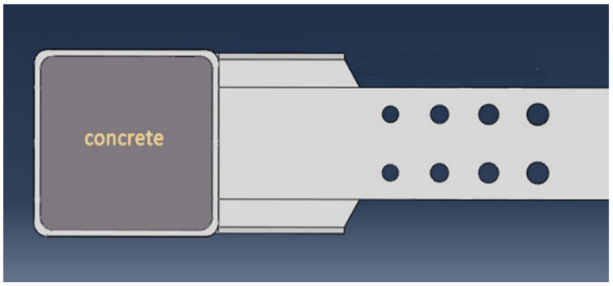

Fig. 4. Drilling with variable diameter on the beam flanges with T-stiffeners.

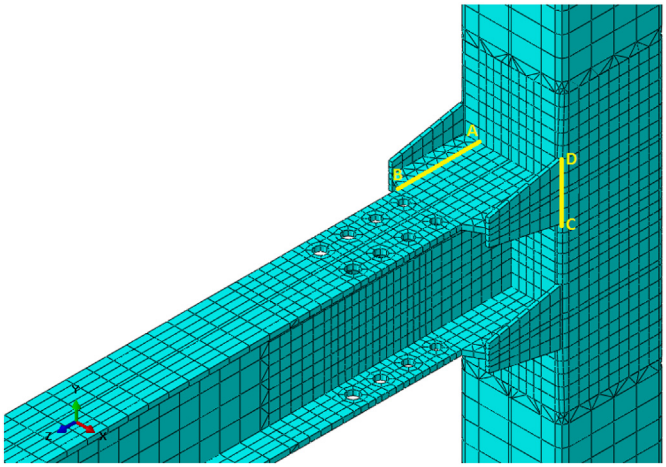

Fig. 5. Lines AB and CD (location of groove welds of stiffener to the beam and column).

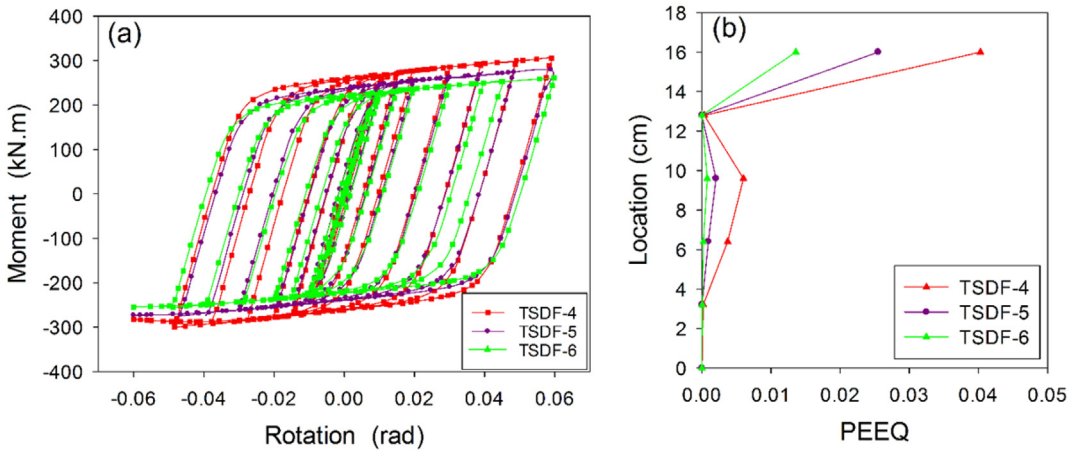

Fig. 6. Effect of hole diameter of beam flange in TSDF-4, TSDF-5, and TSDF-6 models; a) Hysteresis curves; b) equivalent plastic strain at the joint of vertical stiffener to column.

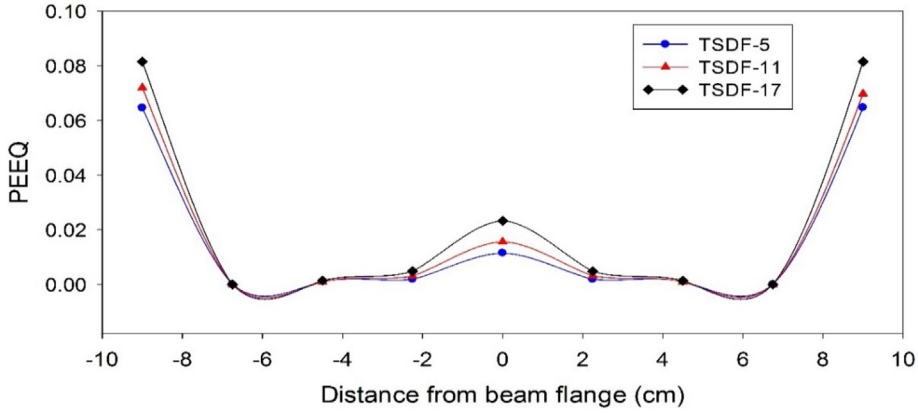

Fig. 7. Effect of distance between holes on the plastic strain reduction in the change location of beam cross-section.

2.5.3. Overall effect of hole drilling on stress concentration

As illustrated in Fig. 8, drilling in the beam flange lead to more uniform stress and strain in the horizontal stiffener groove weld to the beam flange. In addition, the stress in the column face has been greatly reduced by drilling in the beam flange.

2.5.4. Rupture index (RI)

To evaluate more accurately the stress concentration in points B and D at the edge of the horizontal and vertical elements, which are the probable points of crack initiation, the rupture index is studied at these points. Points with higher rupture index are more possible to fracture. The rupture index is calculated using Eq. (2).

$$RI = \frac{\varepsilon_p/\varepsilon_y}{exp\left(-1.5\frac{\sigma_m}{\overline{\sigma}}\right)} \tag{2}$$

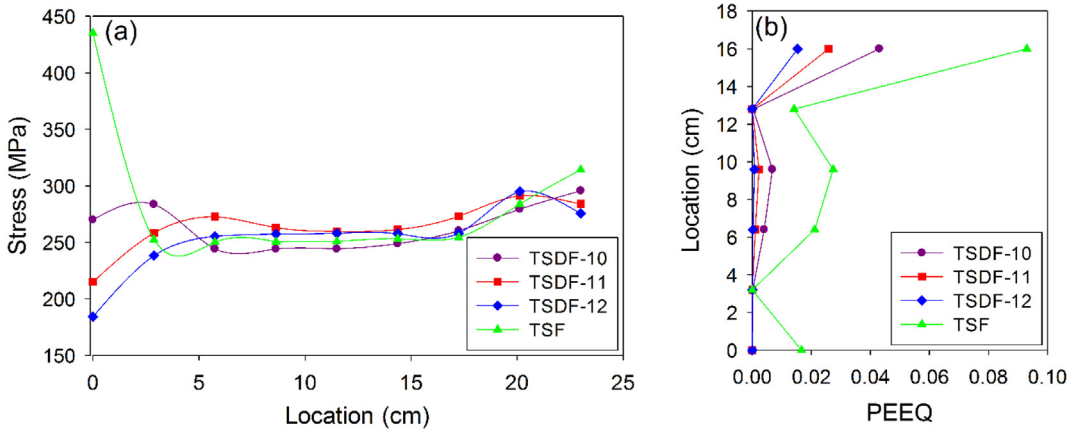

Fig. 8. Stress and strain distribution adjacent the stiffeners; a) stress at the connection joint of horizontal stiffener to beam; b) strain at the connection joint of vertical stiffener to column.

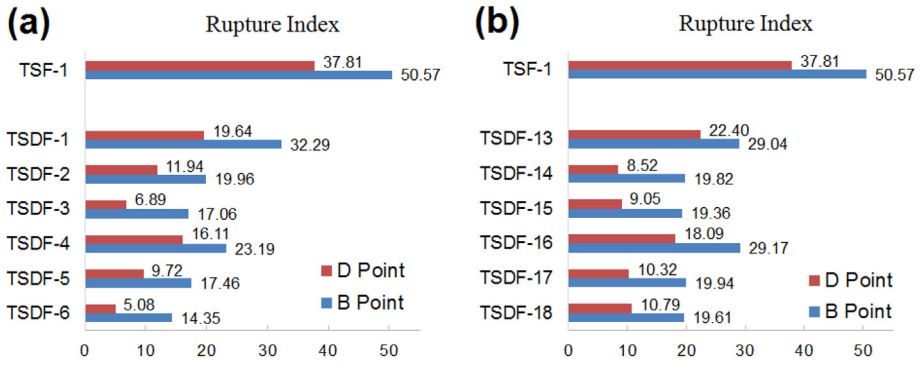

Fig. 9. Rupture index at the horizontal and vertical element edge of stiffener in models; a) b = 210 mm; b) b = 270 mm.

Where, ε_p is the equivalent plastic strain, ε_y is the yield strain, σ_m denotes hydrostatic stress, and $\overline{\sigma}$ is the von Mises equivalent stress. The ratio of $\sigma_m/\overline{\sigma}$ is called triaxiality ratio. The high triaxiality ratio can significantly reduce the failure strain of material and limit its ductility.

As shown in Fig. 9, the rupture index has decreased approximately 50% in the most models in the critical points using hole drilling. Therefore, the probability of brittle failure and the occurrence of crack is decreased at the joint of stiffener groove welds to the beam and column.

2.5.5. Comparison with RBS

In Fig. 10, the equivalent plastic strain of classical RBS is compared with that of TSDF-8 model which has a maximum hole diameter equal to the c parameter of classical RBS. Besides, b parameter of the RBS model is selected the same as the distance of the first and last hole in TSDF-8 model.

As seen in Fig. 10 and the diagram of plastic strain in the connection of stiffeners to the beam and column, it is observed that plastic strain is less in the TSF-1 at the beam axis compared to classical RBS; however, at the groove weld points, the plastic strain is much greater than that of the RBS model. In the TSDF-8 model, by adjusting the hole diameters, the plastic hinge is shifted away from the stiffeners and plastic strains are distributed more uniformly in the beam flange compared to classical RBS. Thus, it avoided concentrated damage and indicated more ductility.

Results showed that the models with variable hole-drilling have a fatter hysteresis curve as well as more energy dissipation, in comparison to the classical RBS model. Fig. 11 shows the hysteresis curves of TSDF-8 model with three holes, TSDF-11 model with four holes, and the RBS model with the similar specifications. As it is observed in Fig. 11, the model with three holes has greater energy dissipation compared to the model with four holes and both hole-drilled models have greater energy dissipation compared to the RBS model.

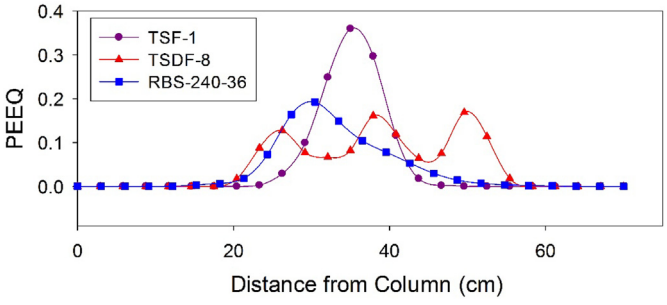

Fig. 10. Comparison of equivalent plastic strain in the hole-drilling models and RBS in the beam flange axis at 0.04 rad.

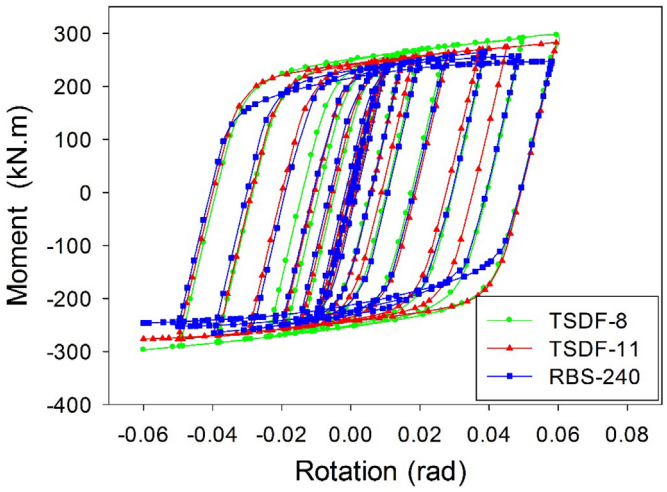

Fig. 11. Comparison of hysteresis curves of models with hole-drilling and classical RBS.

2.6. Hole-drilling with constant diameter

Hole drilling with variable diameters is time consuming and expensive for the reason that it needs to replacement of drill bit for each diameter in common drilling machines. To better fabrication and economization the use of this connection in the building industry, drilling with the constant diameter is proposed. Increasing the number and diameter of holes, leads to increasing the cost of connection. Besides, drilling big holes will be a multistep process for the thick plates.

As noted above, in the second set of models, the application of drilling with constant diameter has been investigated, and in all models, three rows of holes are used. Besides, in the second set of models, stronger beam and stiffener are used for making better use of the column capacity. The thickness and width of the beam flange are 15 mm and 180 mm, respectively and the thickness and height of the beam web are 8 mm and 320 mm, respectively. Fig. 12 schematically shows the second set of analytical models.

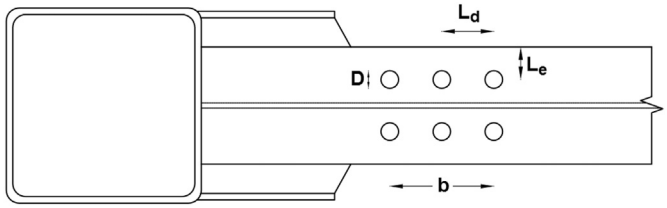

Fig. 12. Parameters used in the second set of analytical models.

Table 5
Hole drilling characteristics of TSDF-19 and TSDF-20 models.

Model	Nomber of holes	D_{min}	D_{max}	b	$\frac{D_{min}}{b_f}$	$\frac{D_{max}}{b_f}$	$\frac{b}{d_b}$
TSDF-19	3	18	27	210	0.10	0.15	0.65
TSDF-20	3	18	27	160	0.10	0.15	0.50

Table 6
Hole drilling characteristics of the second set of analytical models.

Model	b	D	L_e	$\frac{b}{d_b}$	$\frac{D}{b_f}$	$\frac{L_e}{b_f}$
TSDF-21	125	22	43	0.35	0.12	0.24
TSDF-22	125	27	43	0.35	0.15	0.24
TSDF-23	125	32	43	0.35	0.18	0.24
TSDF-24	160	22	43	0.45	0.12	0.24
TSDF-25	160	27	43	0.45	0.15	0.24
TSDF-26	160	32	43	0.45	0.18	0.24
TSDF-27	210	22	43	0.6	0.12	0.24
TSDF-28	210	27	43	0.6	0.15	0.24
TSDF-29	210	32	43	0.6	0.18	0.24
TSDF-30	160	27	47	0.45	0.15	0.26
TSDF-31	160	27	50	0.45	0.15	0.28

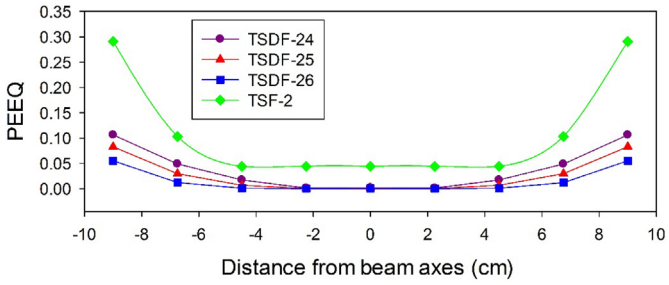

Fig. 13. Comparison of equivalent plastic strain in the location of cross section change for models with and without hole drilling.

Material properties and loading protocol in the second set of models are the same as those of the first set. To compare the first and the second set, two models with varying holes are considered in the second set. The diameter of the biggest hole in these two models is equal to that of two models with the constant diameter. Geometry specifications of the models mentioned above are presented in Table 5. The diameter of holes in the TSDF-19 and TSDF-20 models is 18 mm, 23 mm, and 27 mm.

In these models, D is the hole diameter, b is the distance between the first and last hole, and L_e is the edge distance, which has been shown in Fig. 12. Table 6 shows the characteristics of the other analytical models with the constant diameter. Besides, TSF-2 is a model without holes in the second set of analytical models. It should be noted that in the TSDF-21 up to TSDF-29 models, the holes are located in the middle distance of the beam web and flange edge and the TSDF-30 and TSDF-31 models are generated to study the effect of edge distance.

2.6.1. Effect of D/b_f ratio

As expected, with an increase in the D/b_f ratio, the plastic strain is accumulated around the holes and the strain in the column face decreases. On the other hand, with an increase in hole diameter, moment capacity of connection reduces and the probability of fracture in the holes increases. As illustrated in Fig. 13, drilling of the beam flange extremely reduces the strain concentration at the edges as well as whole section and make it more uniform.

2.6.2. Effect of b/d_b ratio

To study the effect of hole distance on the reduction of stress concentration, the ratio of b/d_b is considered. Fig. 14 shows a comparison of the PEEQ index among the second set of models with b/d_b ratios of 0.35, 0.45, and 0.6. In addition, these ratios are compared with those of hole drilling with different diameters. The PEEQ index is the ratio of equivalent plastic strain to yield strain, which is obtained from Eq. (3).

$$PI = \frac{PEEQ}{\varepsilon_y} \tag{3}$$

As shown in Fig. 14, the PEEQ index in the critical points of the connection initially decreases with an increase in b/d_b ratio and then increases. Minimum PEEQ index is achieved in almost all models for the b/d_b ratio of 0.45. The greater distance of holes result in plastic strain accumulation at the closest hole to the column, and the increase in the probability of rupture at this holes. As it is observed in Fig. 15, in the TSDF-22 model with less hole distance, plastic strain has more uniform distribution and penetrates well in the beam web cross section. The maximum PEEQ in this model is less than that of TSDF-28 model.

2.6.3. Overall effect on stress Concentration

The results of stress on the second set of models are similar to those of the first set and reveal that beam flange drilling significantly reduces the stress concentration at the stiffener horizontal element edge and prevents the occurrence of the brittle failure in this region. Results showed that stress reduces particularly at the column face and becomes more uniform using hole drilling. Besides, out of plane deformation of the column is prevented in this connection. As shown in Fig. 16, beam flange drilling generally results in the reduction of rupture index at points B and D, and causes better proportionality between the horizontal and vertical elements.

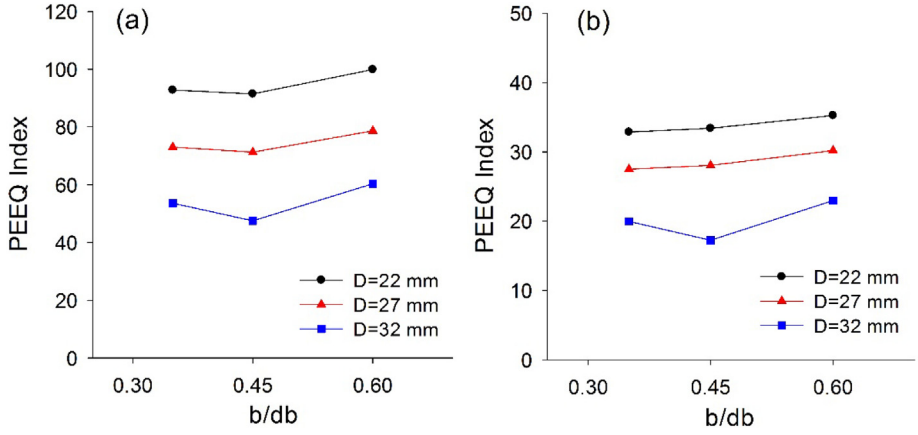

Fig. 14. Effect of hole distance on PEEQ index in the critical points of the stiffener a) point B b) point D.

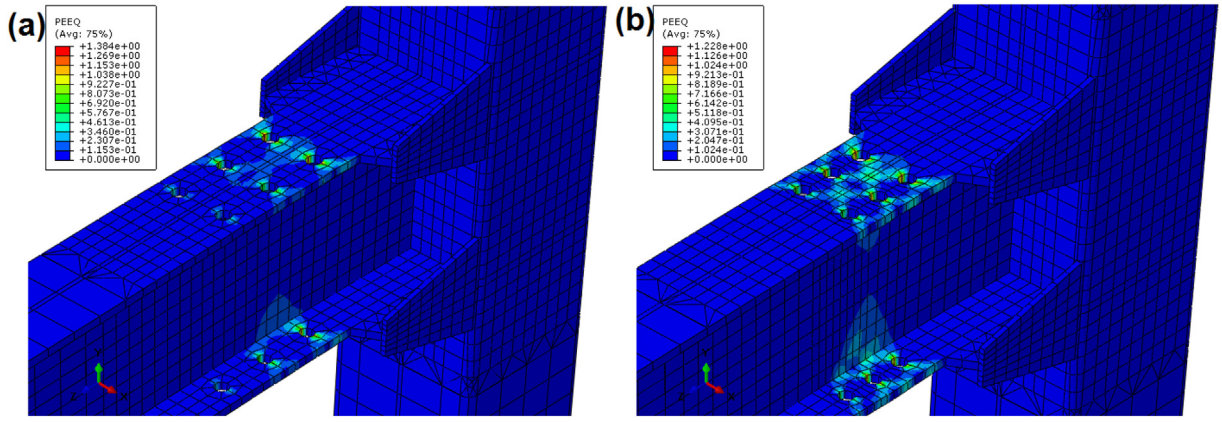

Fig. 15. Effect of hole distance on equivalent plastic strain distribution; a) TSDF-28 model; b) TSDF-22 model.

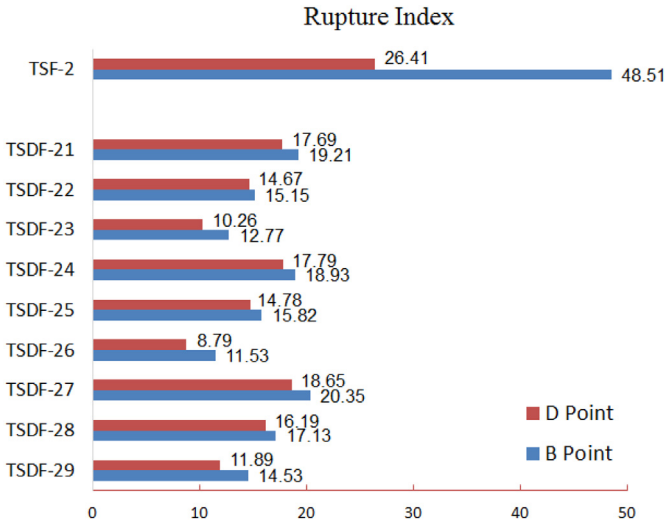

Fig. 16. Rupture index at critical points of the second set of models.

As discussed above, TSDF-24, TSDF-25 and TSDF-26 models show better performance compared to other models with a different b/d_b ratio. In addition, among these three models, TSDF-25 model is the optimum model concerning the moment capacity.

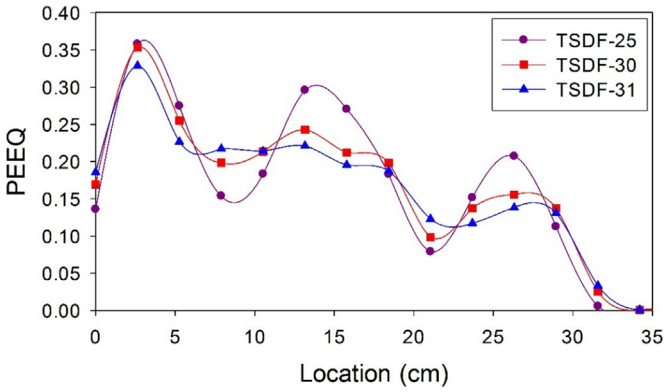

Fig. 18. Equivalent plastic strain at the beam flange edge versus the distance from the edge of horizontal element of stiffener.

2.6.4. Evaluating the fracture and effect of L_e/b_f ratio

Previous investigations had shown that one of the undesirable failure in the drilled beam flange is the fracture of the hole edge, which is considered in this research. As presented in Fig. 17, the TSDF-31 model with L_e/b_f equal to 0.28 has a lower fracture potential compared to other models.

As it is observed in Fig. 18, with an increase in the L_e/b_f ratio, the amount of PEEQ decreases, and a more uniform distribution is found at the beam flange edge resulting in the reduction of fracture potential at the beam flange edge in the direction of hole drilled rows.

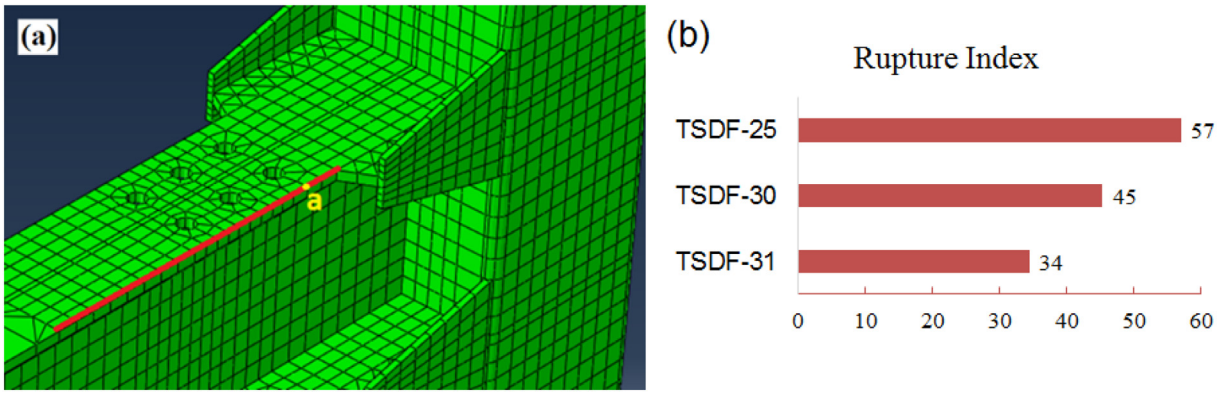

Fig. 17. Effect of edge distance; a) path (red line) and critical point at the beam flange; b) rupture index at point a. (For interpretation of the references to colour in this figure legend, the reader is referred to the web version of this article.)

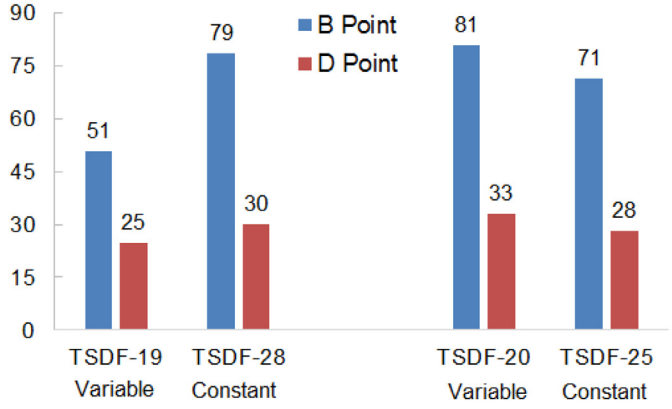

Fig. 19. Comparison of the PEEQ index between hole drilled models with constant and variable diameter.

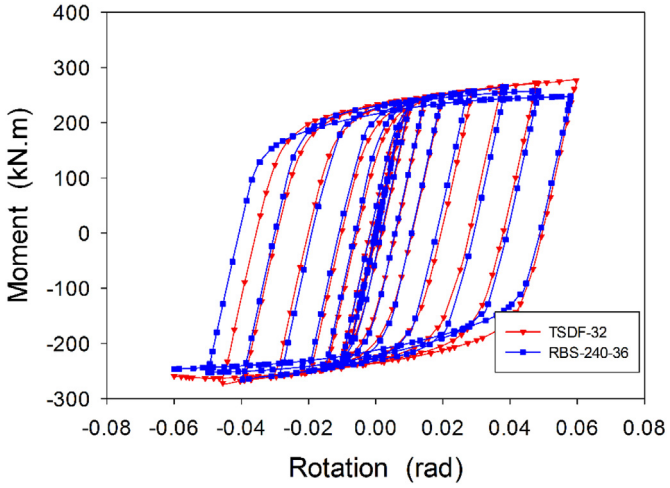

Fig. 20. Hysteresis curves of models with constant holes diameter and classical RBS.

2.6.5. Comparison of hole drilling with constant and variable diameters

The TSDF-19 and TSDF-20 models are modeled and analyzed to compare the results of hole drilling with variable and constant diameters. Fig. 19 shows the diagram of the PEEQ index at critical points of B and D in these models. As it is observed, for the greater value of b/d_b ratios, the model with variable holes has lower stress concentration in critical points; however, at the lower value of b/d_b ratios, the model with constant diameter has lower stress concentration in the critical points of the stiffener connection to the beam and column. However, the model with variable holes shows an overall better performance.

2.6.6. Comparison of hole drilling with constant diameter and classical RBS

In order to compare the behavior of classical RBS model with the RBS model drilled by the constant holes, a new model (TSDF-32 model) with 3-hole row of 36 mm diameter has been generated with the configurations same as TSDF-8 model. Hysteresis curve of TSDF-32 model is shown in Fig. 20. Moreover, the hysteresis curve of classical RBS with c parameter of 36 mm and b parameter of 240 mm (same as the distance between first and third holes of TSDF-32 model) is also depicted in Fig. 20. It can be concluded that energy dissipation of drilled beam with constant hole diameter is very close to that of classical RBS. However, TSDF-32 model has slightly more energy dissipation in the last cycles. This can be due to stress redistribution around the holes.

2.6.7. Comparison of hole drilling with constant diameter and classical RBS

The effect of gravity loads on bending moment diagram is shown in Fig. 21. As shown in this figure, the bending moment on the beam can be decreased in the adjacent of connection [26].

As a result, when the holes with different diameters are used, weaker section takes a major moment and this phenomenon is an undesirable performance. However, since the moment of point 2 is always less than that of point 4, and beam with the reduced section is designed for the maximum moment results of all loading combinations, bending strength will be enough. On the other hand, according to the Mounturi study [26], second plastic hinge in the part that moment is not increasing maybe form in one of the points 1,2 or 3 shown in Fig. 21. Therefore, when used holes are different in their diameters, stress concentration at the weaker section can lead to the formation of second plastic hinge in point 2 that is predefined for acting as a fuse.

3. Experimental Study of the connection

3.1. Experimental Models

To certify the results of analytical models and also evaluate the strength, stiffness, and ductility of the connections, two full scale experimental models were used in this study. Based on the analytical results obtained, and with regard to the main objectives, which include the reduction of stress concentration at the stiffener connection and economic concerns, considering the experimental limitations, one model without hole drilling (TS) and one model with hole drilling at the beam flange (TSDF) were chosen as the experimental models. The hole drilled model is designed based on the TSDF-31 model with regard to the previous experimental studies and the force transmission path in T stiffeners.

The beam and column cross section and also the dimensions and shape of the stiffeners are the same in the experimental models and are similar to the second set of analytical models. Beam and column are selected from plate girder and HSS section, respectively. The design of stiffeners was carried out based on previous researches, and also necessary controls such as seismic compactness of the beam and column section, weak beam-strong column rule, and shear in the panel zone is conducted.

Geometric details of connection components, stiffener dimensions and hole drilling of the beam flange are shown in Fig. 22. In the junction of the stiffeners to the beam and column, the CO_2 welding is used. The yield strength of 4500 (kg/cm^2) with the Charpy V-notch toughness (CVN) of 50 J at $-20\ ^{\circ}C$ were calculated for electrods. Furthermore, the diameter of the used electrode was 1.2 mm. The concrete used was self-compact concrete (SCC) with a compressive strength of 35 MPa.

3.2. Experiment Configuration

The experiment configuration is shown in Fig. 23. The loading method is similar to that of used by Qin et al. [6]. A pinned support is employed at the end of column, and beam end support is considered

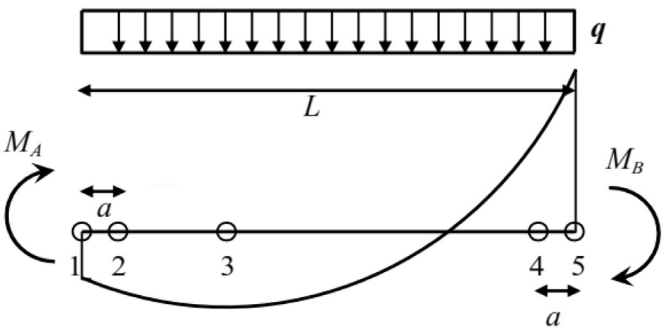

Fig. 21. Total bending moment diagram of beam [26].

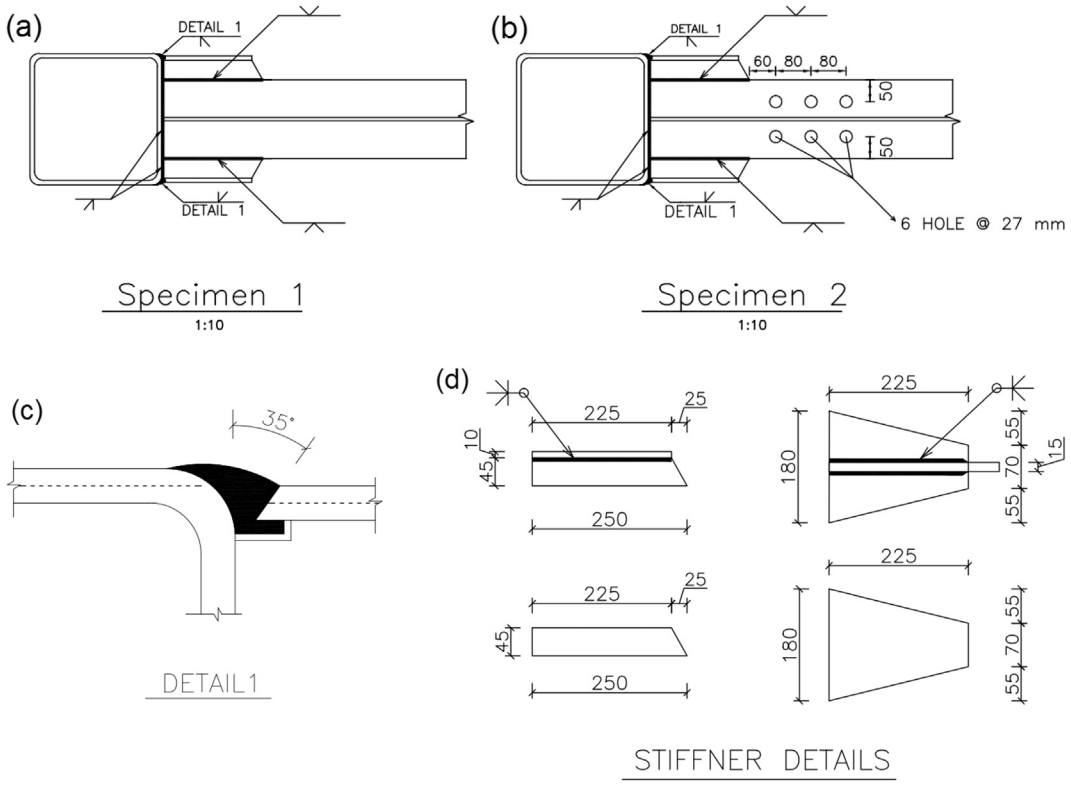

Fig. 22. Details of the horizontal and vertical element of T-stiffener and welding to the column.

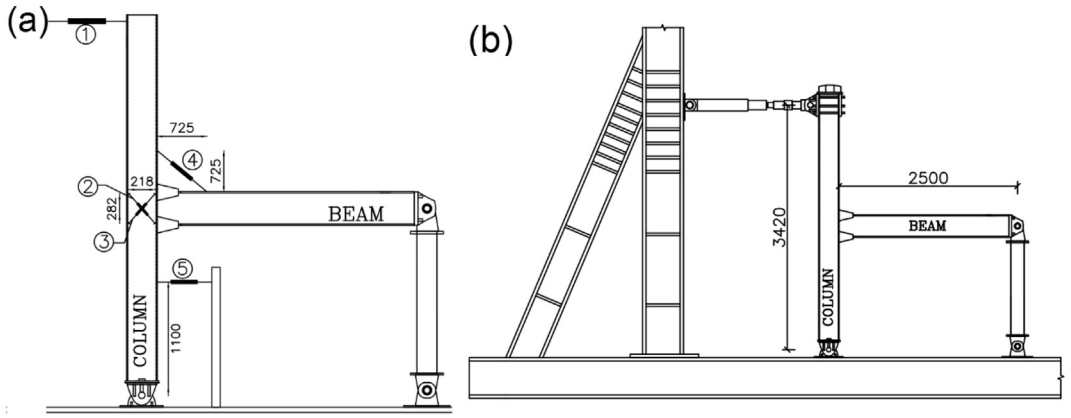

Fig. 23. Configuration of connection models.

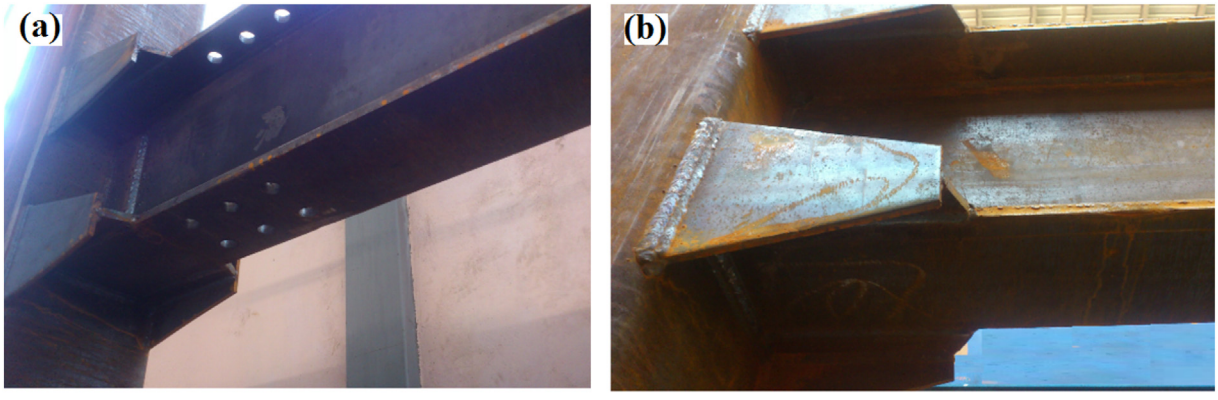

Fig. 24. Experimental models; a) TSDF model; b) TS model.

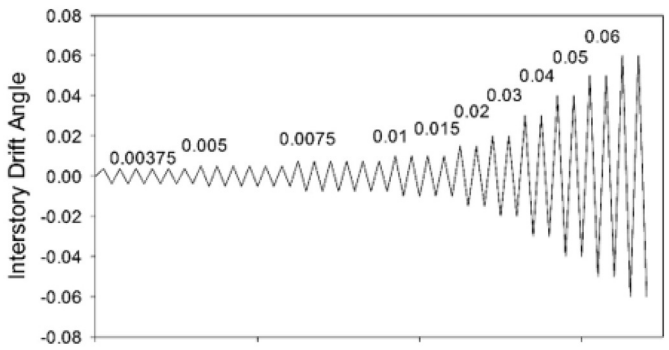

Fig. 25. Loading protocol in the experimental program.

Fig. 27. Deformation of the TS specimen at interstory drift angle of 0.04 rad.

as a roller with appropriate details. Hydraulic actuator is fixed to strong reaction frame and is pinned to the column.

In the top of column, an appropriate roller system is prepared to create a lateral support and prevent out of plane movement of the column. Fig. 24 shows the test specimens. In this study, five LVDT have been utilized to control each specimen. The strain gauges were also used around the holes as well as sensitive points of the test specimens.

3.3. Loading history

The loading history of the experimental program was selected based on the recommendations presented in AISC 341–10 [27] and the SAC/BD-97/02 loading protocol as illustrated in Fig. 25.

The specimens were loaded under displacement control. Displacement of the column end was obtained from multiplying the interstory drift angle by the column height.

3.4. TSDF experimental results

Yielding of the TSDF began from the first hole row at the end of 0.01 rad drift angle. The diagonal yielding pattern was observed similar to numerical analyses at the 0.02 rad drift angle. Moreover, yielding was expanded from the holes to the beam web. At the 0.03 rad drift angle, propagation of whitewash flaking began in the region between the first and second hole rows. Furthermore, yielding was significantly expanded to the last row of hole drilling in the beam flange. According to Fig. 26, no strength degradation was observed up to the end of loading at 0.04 rad drift angle. Stiffeners and their joints to the beam flange and column web were still intact and no yielding was observed in their region.

At the relative drift of 0.05 rad, local buckling of the flange was obviously observed. Strain concentration was almost near the second row of holes. Whitewash flaking was propagated to the horizontal element edge of the stiffener, however, no crack was observed in this area. At the interstory drift angle of 0.06 rad, almost the entire of the beam web was entered into the plastic state. As shown in Fig. 26, the plastic hinge is formed completely far from the column and the stiffeners. Therefore, no significant yielding damage has occurred to the stiffeners and column. To evaluate the potential of fracture at the hole edges due to high local buckling in the flange, loading was continued up to 0.07 rad in this test. Even so, there was no fracture at the area around the holes. Thus, joint rupture is entirely ductile.

3.5. TS experimental results

At the interstory drift angle of 0.01 rad, whitewash flaking began from the joint of the horizontal element to the beam flange. At the interstory drift angle of 0.015 rad, yielding expanded towards the beam end and whitewash flaking was also observed slightly at the beam web. At the interstory drift angle of 0.02 rad, whitewash flaking increased significantly at the location that cross section changes. Observations showed that yielding had greater concentration at the direction of horizontal element edge of T-stiffener.

According to Fig. 27, at interstory drift angle of 0.04 rad, the whitewash flaking expanded towards the column and yielding in the beam web also expanded into the web. Partial strength degradation was observed at the end of loading with the interstory drift angle of 0.05 rad. At interstory drift angle of 0.06 rad, with an increase in stress concentration at the horizontal stiffener edge, specimen experienced sudden fracture at the beam flange. This fracture started at the horizontal element edge of the T-stiffener and quickly was expanded towards the beam axis.

Fig. 28 shows the deformation and ductility condition of the TS specimen at the end of loading 0.06 rad drift angle. The fracture was expanded into the beam web at the end of loading.

3.6. Seismic evaluation of the connection

As illustrated in Fig. 29, in overall condition, hysteresis loops of both specimens are stable and show appropriate ductility and energy dissipation. Based on the American seismic specification for steel

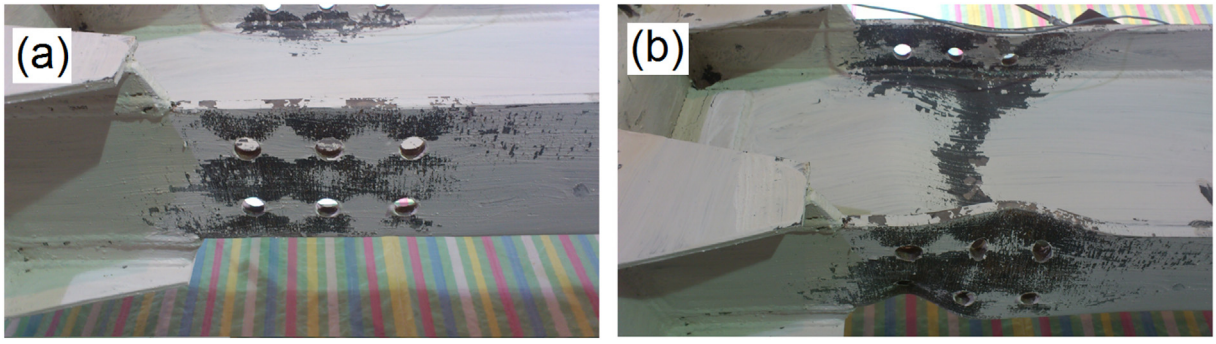

Fig. 26. Connection condition; a) at the interstory drift angle of 0.04 rad; b) at the interstory drift angle of 0.06 rad.

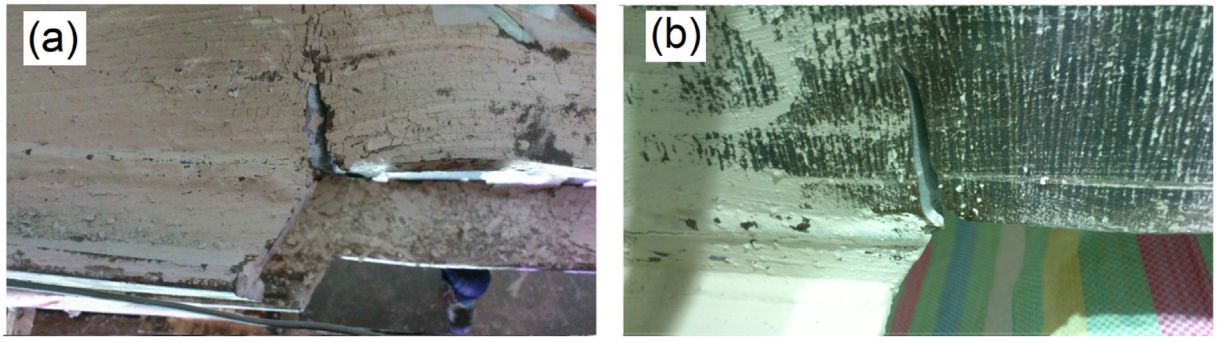

Fig. 28. Deformation of the TS specimen at interstory drift angle of 0.06 rad.

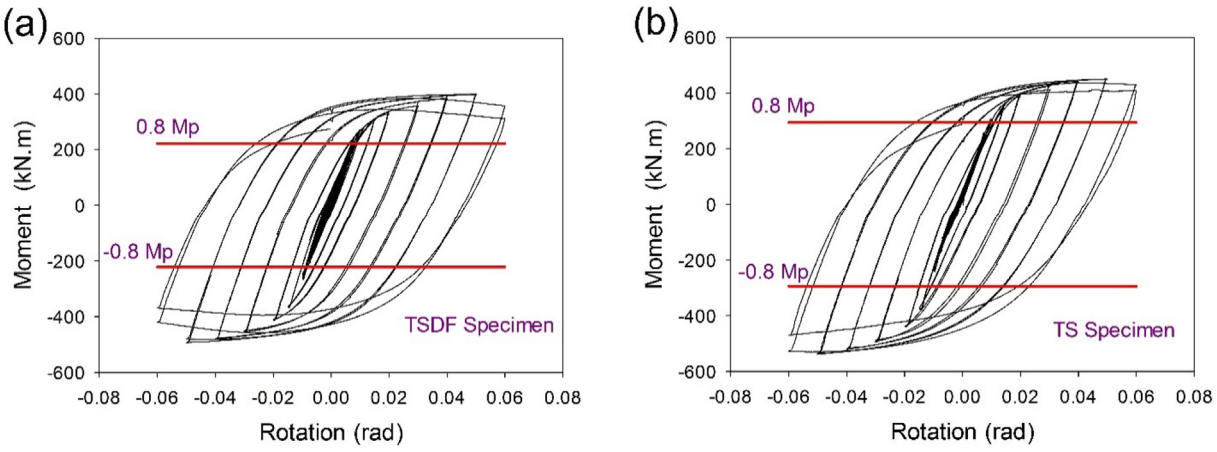

Fig. 29. Hysteresis curves for test specimens; a) TSDF; b) TS.

construction (AISC 318–11), an interstory drift angle of at least 0.04 rad must be sustained by the connection and the measured flexural resistance of the connection shall equal to at least 80% of the plastic moment capacity. Then according to AISC, both specimens are accepted for special moment resisting frames.

Concerning the fact that the TS specimen had severe stress concentration and sudden fracture has occurred in the beam flange at the end of second cycle of loading with interstory drift angle of 0.06 rad and possibly not reliable to undergo the gravity loads. Therefore, this type of connection is not recommended without reducing the beam flange. A comparison between the hysteresis curves of TSDF and TS test specimens in Fig. 30 shows that the stiffness degradation is approximately identical in both specimens. Moreover, the strength degradation of TSDF is gradual while in the TS specimen it occurs almost suddenly. However, the final strength degradation of TS is almost equal to the TSDF specimen.

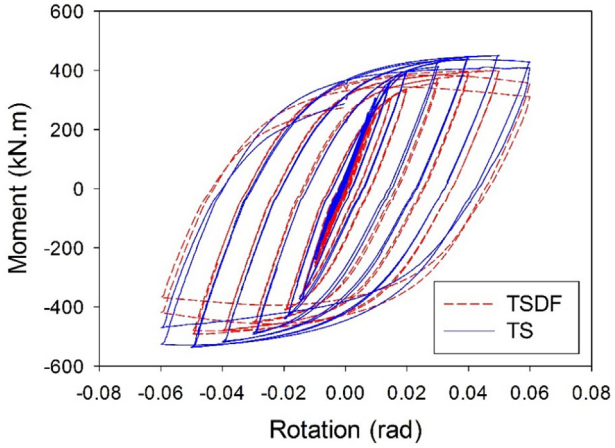

Fig. 30. Comparison of TS and TSDF test specimens.

4. Conclusion

The most important results obtained from this study are outlined below:

1- The rupture index at points with the most stress concentration in finite element analysis decreased over 50% for TSDF-23, TSDF 26 and TSDF 29 in the specimens with constant hole diameter.

2- In the analytical models with variable holes, the equivalent plastic strain (PEEQ) at the joint of stiffener groove welds to beam and column increases with the increase in b/d_b ratio. However, changes in the b/d_b ratio do not have a significant effect on the overall behavior of connection and the hysteresis curve.

3- With an increase of b/d_b ratio in hole drilling with a constant diameter, the rupture index increases at critical points, which is more intense for b/d_b ratios greater than 0.45. While, The PEEQ index for the b/d_b ratio of 0.45 has its least amount and in the models with constant hole diameter, it is less than its value in the variable hole diameter models. In this study, it is recommended that the b/d_b range be considered equal to 0.4 to 0.5.

4- In the test specimens, with an increase in the ratio of L_e/b_f to 0.28, the hole edge fracture was prevented. TSDF specimen was loaded up to a relative drift of 0.07 rad and no fracture was observed at the hole edge or the joint of the stiffener to beam and column.

5- With a decrease in the D_{min}/b_f ratio in the models, the probability of brittle fracture increases in the location of change the cross section. Therefore, the minimum amount of 0.12 in the design of hole drilling with various diameters is proposed.
6- With an increase in hole diameters, stress concentration of T-stiffener groove welds and beam moment capacity decreases. It is suggested that the maximum D_{max}/b_f ratio be limited to 0.2.
7- A comparison of drilled specimens with classical RBS shows that in the first set of drilled specimens with variable diameters, plastic strain compared to RBS is expanded in a more significant length of the beam and strain accumulation is prevented at a point. Furthermore, in these models, local buckling in the beam flange is delayed which cause an increase in the area under the hysteresis curve, energy dissipation and beam stability. However, considering the effect of gravity loads on beam, this result is possibly different and stress, as well as strain, is concentrated in a section. Even so, as explained in this study, this connection has enough strength to sustain against the lateral and gravity loads.
8- Sudden rupture of the TS specimen in the second cycle of 0.06 rad drift angle and flange fracture at this level, compared with the TSDF specimen indicated that hole drilling of the beam flange can be an efficient method for increasing ductility, reducing stress concentration, preventing brittle fracture in this connection and avoiding the rupture in modes 1 and 2 in these connections.
9- Evaluating the PEEQ, TR and IR indices in the analytical and experimental models reveals that these indices can be an excellent criterion for predicting fracture points in these connections.

Acknowledgements

We would like to thank the Neka Foolad Machine Company and its CEO, Eng. Latifi for his financial support in this research project, and granting permission to use the company's equipment.

References

[1] W.L.A. De Oliveira, S.D. Nardin, De Cresce El Debs ALH, Evaluation of passive confinement in CFT columns, J. Constr. Steel Res. 66 (2010) 487–495.
[2] L.H. Han, G.H. Yao, Z. Tao, Performance of concrete-filled thin-walled steel tubes under pure torsion, Thin-Walled Struct. 45 (2007) 24–36.
[3] E. Eiichi Inai, A. Mukai, M. Kai, H. Tokinoya, T. Fukumoto, K. Mori, Behavior of Concrete-Filled Steel Tube Beam Columns, J. Struct. Eng. 130 (2) (2004) 189–202.
[4] Y.M. Alostaz, P. Shneider, Connections to Concrete-Filled Steel Tubes, Eleventh World Conference on Earthquake Engineering (1996) (Paper No. 748).
[5] I.S. Sheet, U. Gunasekaran, G.A. MacRae, Experimental investigation of CFT column to steel beam connections under cyclic loading, J. Constr. Steel Res. 86 (2013) 167–182.
[6] Y. Qin, Z. Chen, Q. Yang, K. Shang, Experimental seismic behavior of through-diaphragm connections to concrete-filled rectangular steel tubular columns, J. Constr. Steel Res. 93 (2014) 32–43.
[7] Y. Yu, Z. Chen, X. Wang, Effect of column flange flexibility on WF-beam to rectangular CFT column connections, J. Constr. Steel Res. 106 (2015) 184–197.
[8] E. Brunesi, R. Nascimbene, G.A. Rassati, Response of partially-restrained bolted beam-to column connections under cyclic loads, J. Constr. Steel Res. 97 (2014) 24–38.
[9] E. Brunesi, R. Nascimbene, G.A. Rassati, Seismic response of MRFs with partially-restrained bolted beam-to-column connections through FE analyses, J. Constr. Steel Res. 107 (2015) 37–49.
[10] R. Nascimbene, An arbitrary cross section, locking free shear-flexible curved beam finite element, Int. J. Comput. Meth. Eng. Sci. Mech. 14 (2013) 90–103.
[11] R. Nascimbene, Towards non-standard numerical modeling of thin-shell structures: geometrically Linear Formulation, Int. J. Comput. Methods Eng. Sci. Mech. 15 (2014) 126–141.
[12] C.H. Kang, K.J. Shin, Y.S. Oh, T.S. Moon, Hysteresis behavior of CFT column to H-beam connections with external T stiffener and penetrate elements, Eng. Struct. 23 (2001) 1194–1201.
[13] K.J. Shin, Y.J. Kim, Y.S. Oh, T.S. Moon, Behavior of welded CFT column to H-beam connections with external stiffeners, Eng. Struct. 26 (2004) 1877–1887.
[14] Y.J. Kim, K.J. Shin, W.J. Kim, Effect of stiffener details on behavior of CFT column to beam connections, Steel Structures 64 (2008) 119–133.
[15] C.H. Kang, Y.J. Kim, K.J. Shin, Y.S. Oh, Experimental Investigation of Composite Moment Connections with External Stiffeners, Adv. Struct. Eng. 16 (10) (2013) 1683–1700.
[16] K.C. Tsai, C.Y. Chen, Performance of ductile steel beam-column moment connections, Eleventh World Conference on Earthquake Engineering (1996) (Paper No. 405).
[17] S.J. Lee, S.E. Han, N.O.H. Se, S.W. Shin, Deformation Capacity of Reduced Beam Section Moment Connection by Staggered Holes, Proceedings of the International Conference on Sustainable Building Asia 2007, pp. 1067–1072.
[18] M.G. Vetr, M. Miri, A. Haddad, Seismic Behavior of a New Reduced Beam Section Connection by Drilled Holes Arrangement (RBS-DHA) on the Beam Flanges Through Experimental Studies. 15 WCEE LISBOA, 2012.
[19] S. Kazerani, N. Fanaie, S. Soroushnia, Seismic behavior of drilled beam section in moment connections, Num. Methods Civil Eng. 1 (2) (2014) 21–28.
[20] K.A.S. Susantha, H.B. Ge, T. Usami, A capacity prediction procedure for concrete filled steel columns, J. Earthq. Eng. 5 (4) (2001) 483–520.
[21] K.J. Shin, Y.J. Kim, Y.S. Oh, Seismic behaviour of composite concrete-filled tube column-to-beam moment connections, J. Constr. Steel Res. 64 (2008) 118–127.
[22] M.S. Ghobadi, M. Ghassemieh, A. Mazroi, A. Abolmaali, Seismic performance of ductile welded connections using T-stiffener, J. Constr. Steel Res. 65 (4) (2009) 766–775.
[23] T.S. Moon, Y.S. Oh, K.J. Shin, C.H. Kang, Hysteresis behavior of CFT column to H-beam connections with external T-stiffeners and penetrated elements, Eng. Struct. 23 (9) (2001) 1194–1201.
[24] ASTM/E8, Standard Test Methods for Tension Testing of Metallic Materials, 2004.
[25] SAC. SAC/BD-97/02 Version 1.1, Protocol for fabrication, inspection, testing, and documentation of beam-column connection tests and other specimens, Sacramento (CA): SAC Joint Venture, 1997.
[26] R. Montuori, The influence of gravity loads on the seismic design of RBS connections, Open Construct. Build. Technol. J. 8 (2014) 248–261.
[27] AISC, ANSI/AISC 341-10. Seismic Provisions for Structural Steel Buildings, American Institute of Steel Construction, Inc., Chicago, IL, 2010.